Available online at www.sciencedirect.com
ScienceDirect
Chemical Physics 341 (2007) 285–295
Chemical Physics
www.elsevier.com/locate/chemphys

Elucidation of population and coherence dynamics using cross-peaks in two-dimensional electronic spectroscopy

Yuan-Chung Cheng, Gregory S. Engel, Graham R. Fleming *

Department of Chemistry and QB3 Institute, University of California, Berkeley and Physical Bioscience Division, Lawrence Berkeley National Laboratory, Berkeley, CA 94720, United States

Received 29 May 2007; accepted 16 July 2007
Available online 10 August 2007

Abstract

In this work, we perform a theoretical study on the dynamics and two-dimensional electronic spectroscopy of a model trimer system and compare the results to experimental data on the Fenna–Matthews–Olson protein. We combine a time-nonlocal quantum master equation formalism and the recently developed method for the efficient calculation of third-order photon echo polarization [M.F. Gelin, D. Egorova, W.J. Domcke, J. Chem. Phys. 123 (2005) 164112] to simulate the 2D electronic spectra of the model system, and compare the time-evolution of the amplitude of cross-peaks to the coherent relaxation dynamics of the system following the excitation by a laser pulse. We show that beats of the upper diagonal peaks in the absolute value 2D spectra provide a direct probe for the coherence dynamics in the system, and the time-evolution of the amplitude of the lower diagonal cross-peaks in the real value 2D spectra can be used to reveal the population transfer among exciton states. Our results verify the intuitive description provided by response functions and demonstrate that the full coherent dynamics in a multichromophoric system can be elucidated using two-dimensional electronic spectroscopy.

1. Introduction

Recent advances in two-dimensional (2D) electronic spectroscopy have generated many new research activities both experimentally and theoretically [1–3]. Experiments performed on laser dye [4–6], *J*-aggregates [7], and photosynthetic light-harvesting complexes [8–10] have demonstrated that the 2D electronic spectroscopy is an effective probe of electronic couplings and dynamical information in the condensed phase. In particular, analysis of 2D lineshape can elucidate the solvation dynamics and solute-solvent interactions for dye and *J*-aggregates in solution [6,7,11,12], while 2D cross-peaks can reveal electronic couplings and energy transfer dynamics in the Fenna–Matthews–Olson bacteriochlorophyll (FMO) complex of green sulphur bacteria [8,13]. Recently, experimental observations of quantum beats in 2D electronic spectra in the FMO complex [10] provided direct evidence of excitonic coherence in the system.

Theoretically, simulations based on exciton models are often used to iteratively fit 2D electronic spectra and provide a model description for the dynamics and electronic couplings in the system [7,9,13]. Because of the complexity of an multichromophoric systems in the condensed phase, these simulations usually require a large number of model parameters, which makes a quantitative fit to the experimental data quite difficult. While these simulations are invaluable for the interpretation of experimental results, it is desirable to have methods that can directly and unambiguously extract quantitative dynamical information from 2D experimental data.

Theoretical studies based on the response function formalism have shown that cross-peaks in 2D electronic spectra are a manifestation of electronic couplings and energy transfer dynamics in a multichromophoric system [14–16]. In addition, quantum beating of cross-peaks arising from excitonic coherence in the system can be related to the coherence dynamics in the system [3,10,17]. In principle,

* Corresponding author.
E-mail address: GRFleming@lbl.gov (G.R. Fleming).

0301-0104/$ - see front matter © 2007 Elsevier B.V. All rights reserved.
doi:10.1016/j.chemphys.2007.07.049

quantitative analysis of the time-evolution of the cross-peaks in 2D electronic spectroscopy should provide a complete understanding of the population and coherence dynamics for the system under study. However, because of possible pulse-overlap effects and interferences between contributions from different Liouville pathways to the signal, it is unclear whether the evolution of cross-peaks can be used to accurately quantify the population and coherence dynamics. Therefore, it is important that we can verify the intuitive description provided by the impulsive response functions and formulate a prescription that can be applied to quantitatively extract dynamical information from experimental 2D spectral data.

In this work, we study the dynamics and 2D electronic spectroscopy of a model trimer system. Based on a time-nonlocal quantum master equation formalism that includes field–matter interaction and non-Markovian effects [18], we study the coherent relaxation dynamics of the system following the excitation by a laser pulse. We also use a recently developed method for the calculation of third-order photon echo polarization [19,20] to simulate the 2D electronic spectra of the model trimer system. Focusing on the time-evolution of the amplitude of cross-peaks, we demonstrate that the population and coherence dynamics of this multichromophoric system can be extracted directly from the time-evolution of the 2D cross-peaks. We close by showing how the ideas presented here apply to the coherence dynamics in the Fenna–Matthews–Olson (FMO) protein of green sulphur bacteria [10,21].

2. Theoretical method

To describe the theoretical method for the calculation of 2D electronic spectra, we first consider a four-wave mixing experiment described in Fig. 1, in which three laser fields interact with the sample to create a polarization that radiates into the phase-matching directions $\pm\mathbf{k}_1 \pm \mathbf{k}_2 \pm \mathbf{k}_3$. For 2D electronic spectroscopy, the signal in the phase-matching direction $\mathbf{k}_s = -\mathbf{k}_1 + \mathbf{k}_2 + \mathbf{k}_3$ is heterodyne-detected and Fourier transformed with respect to the coherence time τ and the rephasing time t to obtain the 2D electronic spectrum at a given population time T [1,2,5].

Theoretically, the 2D electronic spectroscopy is described by the photon echo third-order polarization $P_{\mathrm{PE}}(t)$ in the phase-matching direction $\mathbf{k}_s = -\mathbf{k}_1 + \mathbf{k}_2 + \mathbf{k}_3$. In the standard perturbative approach to nonlinear spectroscopy, $P_{\mathrm{PE}}(t)$ is described by response functions [14]. In the impulsive limit only a subset of the response functions (controlled by enforced pulse ordering) contribute to the signal, enabling intuitive descriptions of the behavior. However, when finite-duration pulses are used, pulse ordering cannot be enforced, complicating the description (and the calculation) significantly. Here we consider a different approach based on a reduced density matrix description of the system that treats the field–matter interactions explicitly, thereby including pulse-overlap effects and contributions from all Liouville pathways in the calculation [19,20].

The time-evolution of the reduced density matrix $\rho(t)$ of a quantum system driven by laser fields can generally be described by a quantum master equation ($\hbar = 1$) [22,23]

$$\dot{\rho}(t) = -\mathrm{i}[H_{\mathrm{S}} + H_{\mathrm{int}}(t), \rho(t)] - \mathscr{R}[\rho(t)], \tag{1}$$

where H_{S} is the Hamiltonian of the electronic system, $H_{\mathrm{int}}(t)$ describes the interaction of the system to the laser fields, and $\mathscr{R}[\cdot]$ represents the dissipative dynamics of the system induced by the system–bath interactions. In this work, the dissipative dynamics of the system is treated by considering a system–bath model in which the electronic system is coupled to a bath of harmonic oscillators. We use the time-nonlocal (TNL, also called time-convolution approach or chronological time ordering prescription) quantum master equation derived by Meier and Tannor [18] to propagate the reduced density matrix and calculate the electronic 2D spectra. Details on the Hamiltonian for the model system and the dissipative environment coupled to the system will be presented in the next section.

In the electric point dipole approximation, $H_{\mathrm{int}}(t)$ can be written as

$$H_{\mathrm{int}}(t) = -\hat{\mu}\mathbf{E}(t), \tag{2}$$

where $\mathbf{E}(t)$ is the time-dependent electric field of the laser pulses, and $\hat{\mu}$ is the transition dipole operator defined in the second-quantized form as

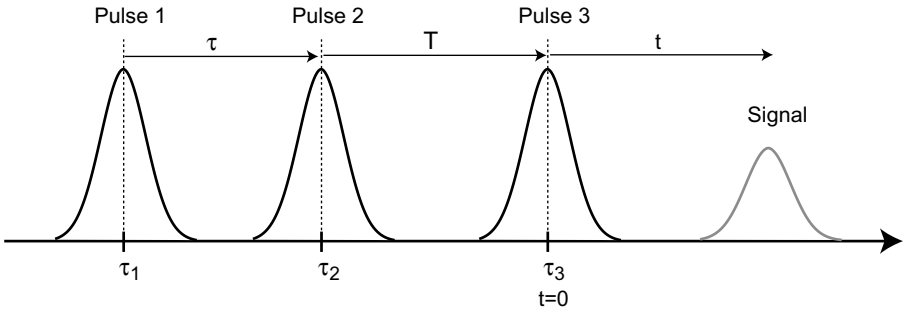

Fig. 1. Three-pulse photon echo experiment and definition of time variables. Three laser pulses centered at τ_1, τ_2, and τ_3 are incident on the sample to generate a signal field. We define the coherence time $\tau = \tau_2 - \tau_1$, the population time $T = \tau_3 - \tau_2$, and the rephasing time t. The pulse sequence depicted here gives positive τ and T. The time zero $t = 0$ is set at the center of the third pulse, τ_3.

$$\hat{\mu} = \sum_n \vec{\mu}_n (a_n + a_n^\dagger), \tag{3}$$

$$= X + X^\dagger. \tag{4}$$

In Eq. (3), a_n ($a_n^\dagger$) is the annihilation (creation) operator that destroys (creates) the nth excitation, and $\vec{\mu}_n$ is the transition dipole moment of the nth excitation. The time-dependent total polarization induced by the laser fields is the expectation value of the transition dipole operator

$$P(t) = \langle \hat{\mu}\rho(t) \rangle, \tag{5}$$

where the bracket $\langle \cdots \rangle$ means taking the expectation value of the operator and averaging over static disorder. When the system–field interaction $H_{\text{int}}(t)$ is explicitly included in the time propagation of $\rho(t)$ (Eq. (1)), the reduced density matrix $\rho(t)$ contains all the information on the time-dependent optical response of the material system. However, to describe a specific experiment in which only signals in a specific phase-matching direction are measured, we need to discriminate against signals in other directions and extract the component that describes the experiment. To this end, we apply the method proposed by Gelin et al. for efficient calculation of the photon echo third-order polarization $P_{\text{PE}}(t)$ [19]. This method has been applied to simulate three-pulse photon echo peak shift and 2D electronic spectroscopy of a two-level electronic system coupled to explicit vibrational degrees of freedom [19,20], and was later extended to treat two-exciton states for describing two-color photon echo peak shift experiments on a bacterial reaction center [24].

Following Gelin et al. [19], we define an operator $P_{\text{e}} = \omega_0 \sum_n a_n^\dagger a_n$, where the sum is over all one-excitation states and ω_0 is a renormalization frequency that can be chosen arbitrarily, and then apply the rotating-wave approximation (RWA) by introducing the reduced Hamiltonian $\overline{H}_{\text{S}} = H_{\text{S}} - P_{\text{e}}$, i.e. all transition frequencies of the one-excitation states are reduced by ω_0. In the RWA, the three laser pulses are described by the time-dependent electric field

$$\mathbf{E}(t) = \sum_{a=1}^{3} [E_a(t-\tau_a) \exp\{-\text{i}(\bar{\omega}_a t - \mathbf{k}_a \cdot \mathbf{r})\} + \text{c.c.}], \tag{6}$$

where $E_a(t-\tau_a)$ is the laser pulse profile, $\bar{\omega}_a$ is the reduced carrier frequency of the field $\bar{\omega}_a = \omega_a - \omega_0$, and $\mathbf{k}_a$ is the momentum. In this work, we adopt a Gaussian pulse profile $E_a(t) \sim \exp(-4\ln 2(t-\tau_a)^2/\tau_{\text{p}}^2)$, where τ_{p} is the pulse duration defined by the full width at half maximum (FWHM) of the pulse profile. Throughout this study, we assume that all three pulses have a $\tau_{\text{p}} = 20$ fs duration and carrier frequency $\omega_a = \omega_0$.

Gelin et al. showed that within the RWA, the third-order polarization in the phase-matching direction $\mathbf{k}_s = -\mathbf{k}_1 + \mathbf{k}_2 + \mathbf{k}_3$ can be calculated by following the time-evolution of three auxiliary density matrices $\rho_1(t) - \rho_3(t)$ defined by the following equations of motion [20]:

$$\begin{aligned}
\partial_t \rho_1(t) &= -\text{i}[\overline{H}_{\text{S}} - V_1(t) - V_2^\dagger(t) - V_3^\dagger(t), \rho_1(t)] - \mathscr{R}[\rho_1(t)], \\
\partial_t \rho_2(t) &= -\text{i}[\overline{H}_{\text{S}} - V_1(t) - V_2^\dagger(t), \rho_2(t)] - \mathscr{R}[\rho_2(t)], \\
\partial_t \rho_3(t) &= -\text{i}[\overline{H}_{\text{S}} - V_1(t) - V_3^\dagger(t), \rho_3(t)] - \mathscr{R}[\rho_3(t)]
\end{aligned} \tag{7}$$

with

$$V_a(t) = E_a(t-\tau_a) \exp(\text{i}\bar{\omega}_a t) X. \tag{8}$$

Eqs. (7) and (8) can be used to propagate the three auxiliary density matrices and calculate the photon echo polarization using

$$P_{\text{PE}}(t) = \langle X(\rho_1(t) - \rho_2(t) - \rho_3(t)) \rangle. \tag{9}$$

Note that $P_{\text{PE}}(t)$ implicitly depends on the coherence time $\tau = \tau_2 - \tau_1$ and the population time $T = \tau_3 - \tau_2$ while $V_a(t)$ depends on the pulse central time τ_a. Eq. (7) is a system of three independent linear differential equations that can be efficiently solved by propagating the auxiliary density matrices. Note that Eqs. (7)–(9) are obtained using a perturbative approach, therefore although the system–field interactions are treated exactly in the equation of motion, the applicability of using Eq. (9) to determine $P_{\text{PE}}(t)$ depends on the optical field being weak. As a result, like the response function approach, the current method is limited to experiments in the weak-field limit.

With the prescription for the calculation of $P_{\text{PE}}(t)$, the 2D Fourier transformed spectrum is then given by double Fourier transform the photon echo polarization field with respect to τ and t:

$$S(\omega_\tau, T, \omega_t) \sim \int \text{d}\tau \int \text{d}t\, \text{e}^{-\text{i}\omega_\tau \tau}\, \text{e}^{\text{i}\omega_t t} \times \text{i}P_{\text{PE}}(\tau, T, t), \tag{10}$$

where ω_τ is the coherence frequency, and ω_t is the rephasing frequency. The 2D signal $S(\omega_\tau, T, \omega_t)$ is a complex function; therefore, it is possible to evaluate the real part, the imaginary part, and the absolute magnitude of $S(\omega_\tau, T, \omega_t)$ at every point. In this work, we will study all three realizations of the 2D spectrum and identify the most useful spectral features to elucidate dynamical information about the system.

Compared to the standard perturbative approach to nonlinear spectroscopy, the present method incorporates all relevant optical fields into the Hamiltonian and propagates the driven dynamics of the system exactly. Therefore, arbitrary pulse shapes and durations can be used in the simulation and pulse-overlap effects and contributions from all applicable Liouville pathways are automatically accounted for. This enables proper simulation of 2D spectra at short population times. More importantly, all relevant dissipative dynamics of the system appear in the calculation. For example, effects of coherent energy transfer and non-Markovian dynamics are included. The dynamical aspect of the method is important, because the method treats the non-Markovian evolution of the density matrix and the third-order polarization in a consistent manner, it allows comparison of the dynamics of the system and the spectral features directly. Note that we do not choose response functions to be included in the simulations, and the dynamics of the system is completely determined by the laser fields and system–bath interactions. This is crucial for the comparative study carried out in this work because it would not be meaningful to study the

dynamics in 2D spectra generated from a prescribed dynamics and the contributions from preselected Feynman diagrams.

3. Model system and dynamics

3.1. Hamiltonian

We study a linear trimer system with nearest-neighbor electronic couplings (Fig. 2) described by a Frenkel-exciton model with three two-level chromophores:

$$H_S = \varepsilon_g|0\rangle\langle 0| + \sum_{n=1}^{3} \varepsilon_n a_n^\dagger a_n, \tag{11}$$

$$+ J_{12}(a_1^\dagger a_2 + a_2^\dagger a_1) + J_{23}(a_2^\dagger a_3 + a_3^\dagger a_2), \tag{12}$$

where $|0\rangle$ denotes the electronic ground state, a_n ($a_n^\dagger$) is the annihilation (creation) operator that destroys (creates) an excitation at site n, ε_g is the energy of the ground state, ε_n is the site energy at the nth chromophore, and J_{nm} is the electronic coupling between the n and mth chromophores. This model is an extension of the extensively studied dimer model and can be used to model systems with energy transfer or charge transfer through a bridge state. a_n and $a_n^\dagger$ describe electronic transitions between the molecular ground and excited states, and they satisfy the Pauli commutation relations

$$[a_n, a_m^\dagger] = \delta_{nm}(1 - 2a_n^\dagger a_n), \quad [a_n, a_m] = 0. \tag{13}$$

The total system-plus-bath Hamiltonian is

$$H_T = H_S + H_{int}(t) + H_B + H_{SB}, \tag{14}$$

where $H_{int}(t)$ is the system–field interactions defined in Eqs. (2) and (3), H_B is the bath Hamiltonian, and H_{SB} describes the system–bath interaction. Explicit inclusion of the system–field interactions allows us to treat the driven dynamics of the system exactly and use the result to compute the third-order polarization. For the system–bath interactions, we assume a harmonic bath of independent harmonic oscillators for H_B, and the electronic system is coupled linearly and diagonally to the bath through a number of collective bath coordinates:

$$H_{SB} = -\sum_{n=1}^{3} a_n^\dagger a_n \cdot q_n, \tag{15}$$

where q_n denotes a collective bath coordinate that is coupled to the nth chromophore in the system. Such excitation-bath couplings induce diagonal transition energy fluctuations in the site-representation. For simplicity, we assume that the bath coupled to each chromophore is described by the same Ohmic spectral function with an exponential cut-off

$$J(\omega) = \gamma_0 \omega \exp(-\omega/\omega_c),$$

where γ_0 is the coupling strength and ω_c is the cut-off frequency of the bath. We also assume that baths coupled to different system operators are independent, i.e., the correlation function $C_{nm}(t) = \langle q_n(t) q_m(0)\rangle$ is zero when $n \neq m$.

In addition, to properly describe the third-order polarization, it is necessary to include contributions from the two-excitation states. To this end, we use the exciton commutation rule in Eq. (13) to expand all system operators in the ground and one-excitation subspace to the two-excitation manifold. This allows treatment of excitonic dynamics in the one- and two-excitation subspace in a consistent manner [24]. For example, the exciton Hamiltonian in Eq. (11) can be represented in the full Hilbert space, and the diagonalization of the full matrix will result in manifolds of a ground state, three one-exciton states (called e_1, e_2, and e_3 from low energy to high energy in this work), and three two-exciton states.

In this work, we study a linear trimer system with nearest-neighbor couplings $J_{12} = J_{23} = 100\ \text{cm}^{-1}$, and with site energies of each chromophore relative to the renormalization frequency ω_0 given by $E_1 = -50\ \text{cm}^{-1}$, $E_2 = 0\ \text{cm}^{-1}$, and $E_3 = 50\ \text{cm}^{-1}$. In the exciton representation, the three excitonic states e_1, e_2, and e_3 have relative energies of $-150\ \text{cm}^{-1}$, $0\ \text{cm}^{-1}$, and $150\ \text{cm}^{-1}$, respectively. Effectively, we choose to set the laser carrier frequency ω_0 to be on resonance with the e_2 exciton state and apply the RWA so that all transition frequencies are reduced by ω_0. The bath parameters for the model system are $\gamma_0 = 0.7$ and $\omega_c = 150\ \text{cm}^{-1}$, and all the simulations are carried out at 77 K. This corresponds to weak system–bath coupling so that the TNL quantum master equation based on weak coupling approximation is applicable. Static disorder is ignored in this work. Because our focus in this work is on the time-evolution of the amplitude of 2D cross-peaks, rather than the 2D lineshape of the peaks, we expect the neglect of static disorder to have minor effect to the results in this work.

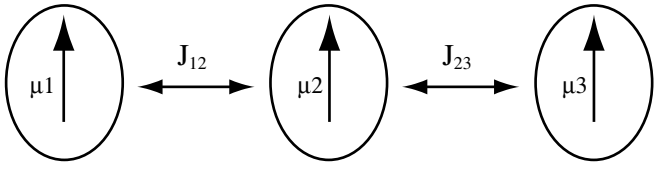

Fig. 2. Model linear trimer system. We studied a linear trimer system with nearest-neighbor coupling J_{12} and J_{23}. In this work, $J_{12} = J_{23} = 100\ \text{cm}^{-1}$ are used, and the site energies of each chromophore relative to the carrier frequency of the laser ω_0 are $E_1 = -50\ \text{cm}^{-1}$, $E_2 = 0\ \text{cm}^{-1}$, and $E_3 = 50\ \text{cm}^{-1}$, respectively. In the exciton representation, the three excitonic states have relative energies of $-150\ \text{cm}^{-1}$, $0\ \text{cm}^{-1}$, and $150\ \text{cm}^{-1}$, respectively. The transition dipole of the three chromophores are assumed to be parallel to each other and the transition dipole strengths are $\mu_1 = 5$ and $\mu_2 = \mu_3 = 1$. A Ohmic bath with $\gamma_0 = 0.7$ and cut-off frequency $\omega_c = 150\ \text{cm}^{-1}$ is used for all three chromophores. The temperature is set to 77 K.

3.2. Dynamics

With the system–bath Hamiltonian and the bath spectral density, we calculate the driven dynamics of the reduced density matrix of the system $\rho(t)$ using the non-

Markovian time-nonlocal (TNL) quantum master equation derived by Meier and Tannor [18]. Unlike the Redfield theory [22], this formulation of the quantum master equation includes non-Markovian dynamics and bath memory effects. In this section, we briefly describe the dynamics of the system following the optical excitation by the 20 fs laser pulse calculated using the TNL quantum master equation. In our simulation, we numerically propagate the TNL dynamics using an iterated Crank–Nicholson scheme [25]. The results in this section serve as a benchmark for our study of the 2D electronic spectroscopy in the next section.

In Fig. 3, we show the time-evolution of the one-exciton density matrix elements in the exciton representation when the model trimer system is initially in the ground state and excited by the 20 fs laser pulse at time $t = 0$. The time-evolution of the diagonal density matrix elements (population) and off-diagonal density matrix elements (coherence) of the model trimer system are shown. The short laser pulse excites all three exciton states and creates optical coherence represented by nonzero coherence elements in the density matrix. The subsequent time-evolution of the density matrix exhibits population transfer and coherence dynamics (dephasing and coherence transfer). In Fig. 3a, we also show that the population dynamics can be reasonably described by a three-state sequential kinetic model including 150 fs $e_3 \rightarrow e_2$ transfer and 180 fs $e_2 \rightarrow e_1$ transfer (thin-dashed curves in Fig. 3a). The three coherence density matrix elements (Fig. 3b) clearly decay in a time scale comparable or longer than the population transfer time scales. We expect these population dynamics and coherence dynamics to manifest themselves in the 2D electronic spectra. In the next section, we will numerically simulate 2D electronic spectra for the model trimer system and demonstrate that the full dynamics of the density matrix presented in this section can be elucidated from the time-evolution of 2D cross-peaks.

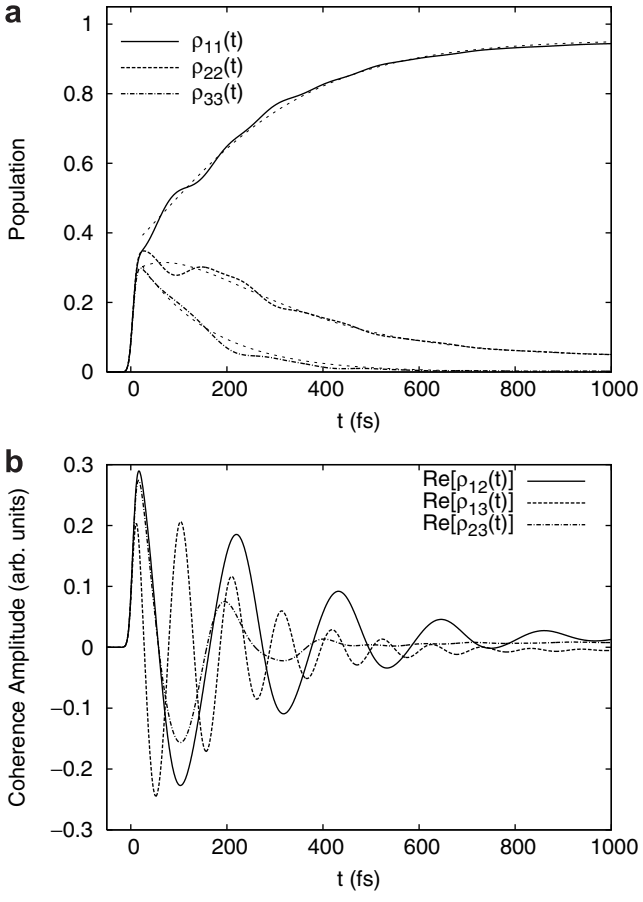

Fig. 3. Dynamics of the model trimer system in the exciton representation. We show the time-evolution of the diagonal density matrix elements (upper) and the real parts of the off-diagonal density matrix elements (lower) when the model trimer system is excited by a 20 fs laser pulse on resonance with the e_2 exciton state. The population dynamics generated by a kinetic model including 150 fs $e_3 \rightarrow e_2$ transfer and 180 fs $e_2 \rightarrow e_3$ transfer is shown in thin-dashed lines. The population dynamics is well reproduced by the kinetic model.

It is also instructive to consider the population dynamics in the site-representation to understand how the excitation moves in space. In Fig. 4, we show the population dynamics in the site-representation. Because site 1 has the strongest transition dipole strength, the laser excitation localizes the initial population it generates mostly on this site. The subsequent dynamics thus represents excitation redistribution in space. The population transfer in the site-representation exhibits prominently coherent oscillatory motions; that is, the energy transfer is described by wave-like coherent motion, rather than incoherent hopping from one site to the other. This behavior is expected in this parameter regime because the electronic coupling is stronger than the site energy difference and the system–bath coupling is relatively weak. As a result of the reversible population transfer, the population on site 3, representing the population transferred from one end of the linear trimer system to the other end of it, reaches values greater than the equilibrium population at short times. Imagine an energy trap is present close to site 3 and is able to efficiently remove population from this site; the system would exhibit an enhanced efficiency of energy trapping because

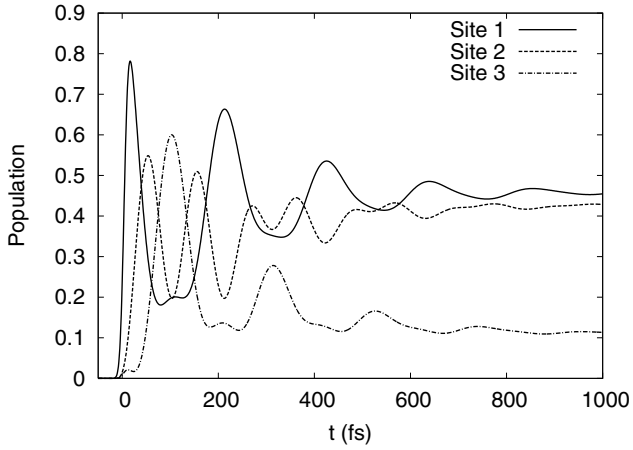

Fig. 4. Population dynamics in the site-representation. The population redistribution exhibits reversible wave-like motion, showing the coherent nature of the energy relaxation.

of the excitonic coherence. Similar coherent transport models have been studied theoretically as models of efficient energy trapping in photosynthetic light-harvesting systems [26]. In addition, recent experimental observations of long-lasting excitonic coherence in photosynthetic complexes suggest coherent energy transfer in photosynthetic systems [10,27]. It is possible that these coherent population motions in space is responsible for the efficient energy trapping in photosynthesis.

4. Results and discussion

To simulate the 2D electronic spectra for the model trimer system, we apply the TNL quantum master equation to propagate Eqs. (7) and (8) and calculate the photon echo polarization $P_{\mathrm{PE}}(\tau, T, t)$ according to Eq. (9). For the 2D electronic spectrum at a given population time T, we compute $P_{\mathrm{PE}}(\tau, T, t)$ on a two-dimensional grid of coherence time (τ) and rephasing time (t) points and then perform numerical fast Fourier transform on the 2D grid according to Eq. (10) to obtain the complex 2D signal $S(\omega_\tau, T, \omega_t)$ in the frequency domain. The amplitude of a peak defined as the volume underneath a rectangular area surrounding the peak is calculated using the 2D Simpson rule to numerically integrate over the area on the 2D electronic spectra.

Fig. 5 shows the simulated real value 2D electronic spectra of the model system at population times $T = 0$, 100, 300, and 600 fs. At $T = 0$, three diagonal peaks can be resolved and assigned to the three exciton states, e_1, e_2, and e_3, respectively, from low to high energy. In addition, cross-peaks are clearly observable in the $T = 0$ spectrum, indicating excitonic couplings and correlation among exciton states. The negative feature at the upper diagonal e_1, e_2 cross-peak can be attributed to the excited state absorption from an initially excited $|e_1\rangle\langle e_1|$ population. The beat of this cross-peak in T is due to excitonic coherence and can be clearly seen. Moreover, as the population time, T, increases, the diagonal peaks and lower diagonal cross-peaks evolve, showing population dynamics in the system. The negative feature at the e_2, e_2 diagonal peak that appears in 600 fs results from the excited state absorption contributions when the initially created population state undergoes population transfer to another one-exciton state during T. More detailed dynamical information can be obtained by following the amplitude of an individual peak as a function of T.

We will now focus on the amplitude of the cross-peaks. An intuitive way to think about the peaks in the 2D electronic spectrum is to consider the impulsive response functions that contribute to the signal. In Fig. 6, we show the Liouville pathways that are expected to contribute to a

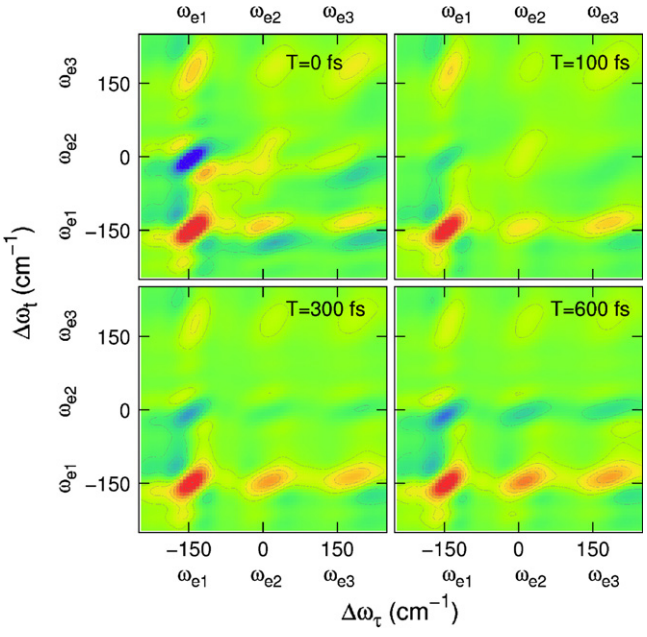

Fig. 5. Simulated 2D electronic spectra for the model system at $T = 0$, 100, 300, and 600 fs. The x- and y-axis are respectively the coherence frequency and the rephasing frequency relative to the carrier frequency of the laser ω_0. The relative transition energies of the three exciton states are at $-150\ \mathrm{cm}^{-1}$, $0\ \mathrm{cm}^{-1}$, and $150\ \mathrm{cm}^{-1}$, respectively.

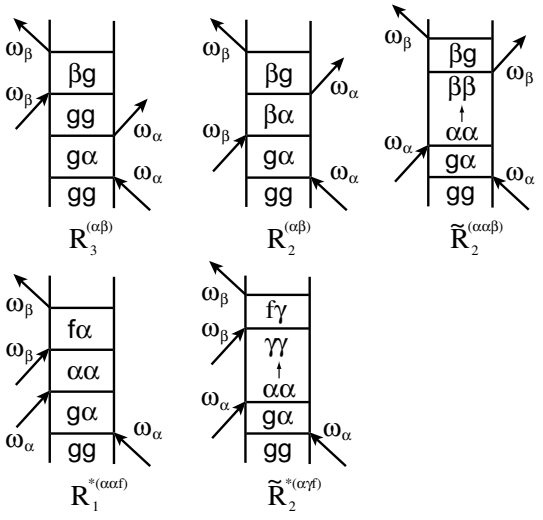

Fig. 6. Double-sided Feynman diagrams representing the Liouville pathways contributing to a cross-peak at $(\omega_\alpha, \omega_\beta)$. In these diagrams, g denotes the ground state, the Greek letters denote one-exciton states, and f represents a two-exciton state. The $R_2^{(\alpha\beta)}$ term represents a pathway in which the system is in a coherence state $|\alpha\rangle\langle\beta|$ during the population time T, therefore, an oscillating phase factor with a frequency of $\Delta E_{\alpha\beta}$ is associated with this term. All other terms do not exhibit such excitonic oscillation in the population time because the system is in a population state during the population period. The $\tilde{R}_2^{(\alpha\alpha\beta)}$ term represents the energy transfer contributions when the initial population state $|\alpha\rangle\langle\alpha|$ undergoes population transfer into $|\beta\rangle\langle\beta|$ during T. Because the uphill population transfer is negligible at low temperatures, we expect the $\tilde{R}_2^{(\alpha\alpha\beta)}$ term contributes to the lower diagonal cross-peaks, rather than upper diagonal cross-peaks. The $R_1^{*(\alpha\alpha f)}$ term represents the excited state absorption contributions from the initial population state $|\alpha\rangle\langle\alpha|$, and the $\tilde{R}_2^{*(\alpha\gamma f)}$ term represents the excited state absorption contributions when the initially created population state transfers to another one-exciton state during T. The two excited state absorption pathways have negative contribution to the total response function, therefore they generate negative features in the real value 2D electronic spectra.

cross-peak at the $(\omega_\alpha, \omega_\beta)$ position. Our simulation is, however, not based on the response function formalism, and thus not limited to the contributions from these Liouville pathways alone. Nevertheless, these diagrams provide a convenient way to think about the main contributions to the cross-peak. The impulsive response function that primarily determines the amplitude of the cross-peak at the position $(\omega_\alpha, \omega_\beta)$ is [3]

$$R(T) = R_3^{(\alpha\beta)}(T) + R_2^{(\alpha\beta)}(T) + G_{\beta\alpha}(T)\widetilde{R}_2^{(\alpha\alpha\beta)}(T) - G_{\alpha\alpha}(T)R_1^{*(\alpha\alpha f)}(T) - G_{\gamma\alpha}(T)\widetilde{R}_2^{*(\alpha\gamma f)}(T), \quad (16)$$

where $G_{\beta\alpha}(t)$ is the conditional probability of finding the system in the $|\beta\rangle\langle\beta|$ population state at time t when the system is initially in the $|\alpha\rangle\langle\alpha|$ population state at $t = 0$. These conditional probability terms describe the effects of population transfer. The $R_2^{(\alpha\beta)}$ term represents the coherence pathway in which the system is in a coherence state $|\beta\rangle\langle\alpha|$ during the population time T. Because the time-evolution of the coherence state has an oscillating phase factor with the frequency equal to the energy difference between the pair of exciton states ($\omega_{\alpha\beta} = E_\beta - E_\alpha$), the $R_2^{(\alpha\beta)}$ contribution causes excitonic quantum beats in the 2D spectra [16]. This picture based on the impulsive response functions is an over-simplified one, and our simulated 2D spectra actually contain contributions from pulse-overlap effects and additional Liouville pathways. Nevertheless, we find the simple response function picture provides us a convenient way to interpret our results.

4.1. Upper diagonal cross-peaks at coherence frequency $\omega_\tau = \omega_{e1}$

We will now use the intuitive picture developed above to study the population time-evolution of the amplitude of cross-peaks for the 2D spectra of the model system, focusing on spectral evolutions that can be used to extract population and coherence dynamics directly from the simulated 2D spectra. We first study the time-evolution of the upper diagonal cross-peaks related to the lowest exciton state e_1 (with coherence frequency ω_{e1}). These cross-peaks are generated when the first pulse interacts with the e_1 state of the system and in the end the system radiates a field at the ω_{e2} (the e_1, e_2 cross-peak) or ω_{e3} (the e_1, e_3 cross-peak) frequency. Because the e_1 state is the lowest energy state and the uphill population transfer is negligible at 77 K, the energy transfer pathways $\widetilde{R}_2^{(\alpha\alpha\beta)}$ and $\widetilde{R}_2^{*(\alpha\gamma f)}$ do not contribute to these cross-peaks, and similarly, the contributions from the excited state absorption pathway $R_1^{*(\alpha\alpha f)}$ do not affect the long time behavior of the cross-peaks. As a result, we expect these peaks to be free of interferences from population dynamics and to provide a direct probe of the coherence dynamics.

In Fig. 7, we show the time-evolution of the amplitude of these upper cross-peaks. The amplitude of the real part, the imaginary part, and the absolute value of the peaks are shown as a function of the population time T. In general,

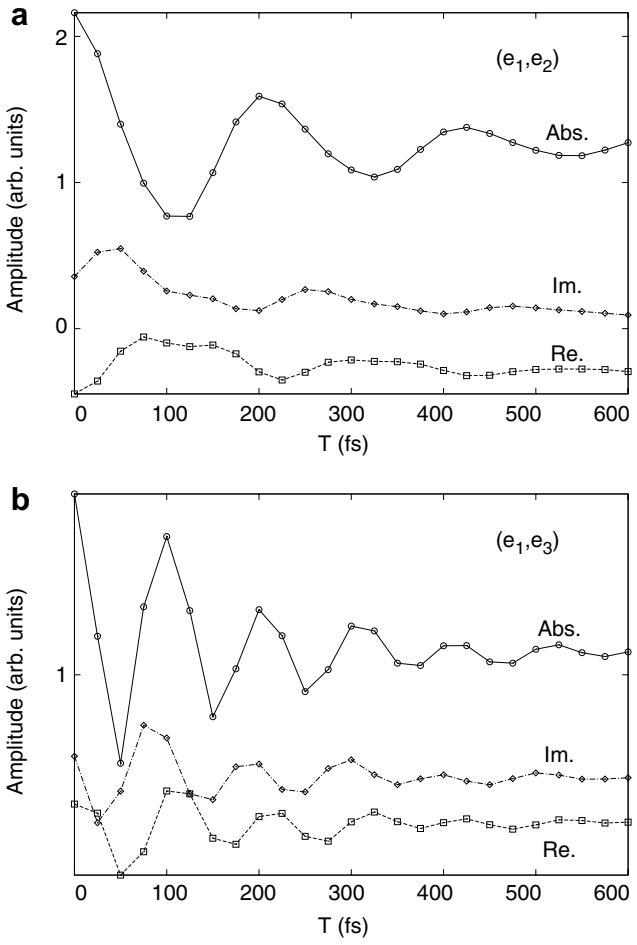

Fig. 7. Population time-evolution of upper diagonal 2D cross-peaks involving the e_1 exciton state. The real part (square), imaginary part (diamond), and absolute value (circle) amplitude of the e_1, e_2 and e_1, e_3 cross-peaks in the 2D spectrum as a function of population time T are shown. The pronounced beats in the absolute value peak amplitude are due to the contributions from the $R_2^{(\alpha\beta)}$ pathway.

while the real and imaginary amplitudes of the cross-peaks do show quantum beats, the beating patterns are obscured because of the interferences from the T dependence of the response functions. In contrast, the absolute value peak amplitude exhibits clear oscillatory behavior. The prominent beats in the amplitude of the absolute value cross-peaks indicate that the T dependence of the response functions contributing to these upper diagonal cross-peaks are described by a common phase factor which vanishes in the absolute value spectra, except for the $R_2^{(\alpha\beta)}$ coherence term which has an excitonic phase factor.

In Fig. 8, we compare the oscillatory part of the absolute amplitude of these upper diagonal cross-peaks to the dynamics of the corresponding off-diagonal density matrix elements calculated directly from the time-nonlocal quantum master equation upon the excitation by a laser pulse at time $t = 0$ (Section 3.2). We find excellent correlation between the oscillatory part of the absolute amplitude and the real part of the coherence density matrix elements. This result indicates that the beat of the absolute amplitude

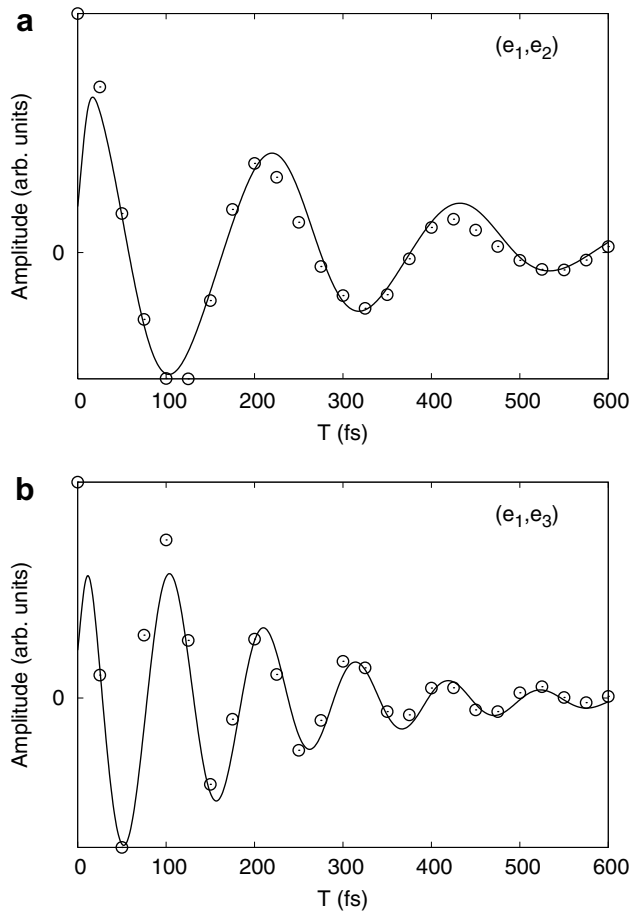

Fig. 8. A comparison between the coherence dynamics (solid line, scaled) and the absolute amplitude of 2D cross-peaks as a function of population time T. The excellent agreement indicates that beats in the absolute amplitude of these upper diagonal cross-peaks are a direct probe of the coherence dynamics.

of an upper diagonal cross-peak can be used as a direct measure of the coherence dynamics. The time-evolution of the absolute amplitude of the e_1, e_2 cross-peak is described by a damped 155 cm^{-1} oscillation with 215 fs exponential decay time, which can be assigned to the dephasing time of the $|e_1\rangle\langle e_2|$ coherence. The time-evolution of the absolute amplitude of the e_1, e_3 cross-peak is described by a rapid 60 fs exponential decay and a damped 320 cm^{-1} oscillation with 150 fs decay time that can be attributed to the dephasing time of the $|e_1\rangle\langle e_3|$ coherence. The 60 fs decay can be attributed to bath relaxation.

Our simulations indicate that the beats of the absolute amplitude of upper diagonal cross-peaks directly and quantitatively reflect the coherence dynamics in the system. This result is not trivial because in general bath relaxation and other dynamical effects could also affect the time-evolution of the cross-peaks, and a complex phase factor can exist in the coherence dynamics that is not captured by the oscillatory part of the absolute value amplitude. Clearly, in this model system, the bath memory effects only have minor contribution to the absolute magnitude of the upper diagonal cross-peaks. Simulations were also performed on trimer systems with different site energies, electronic couplings, and off-diagonal system–bath couplings, and similar trends were observed. Therefore, this observation should be applicable to more general systems.

4.2. Lower diagonal cross-peaks at rephasing frequency $\omega_t = \omega_{e1}$

In contrast to the upper diagonal cross-peaks, the lower diagonal cross-peaks contain contributions from energy transfer pathways. In Fig. 9, we show population time-evolution of the lower diagonal e_2, e_1 and e_3, e_1 cross-peaks. These cross-peaks are generated when the first pulse interacts with either the e_2 or e_3 exciton state of the system and the system subsequently radiates at the ω_{e1} frequency. Clearly, the amplitude of these lower diagonal cross-peaks exhibit a damped oscillatory component due to the $R_2^{(\alpha\beta)}$ coherence pathway contributions and a rise component

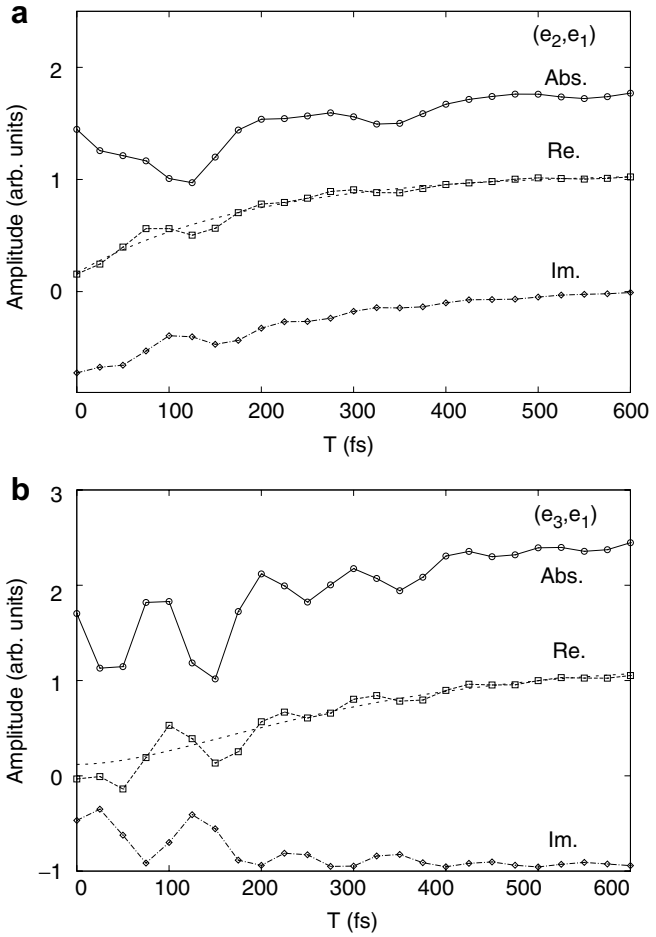

Fig. 9. Population time-evolution of lower diagonal 2D cross-peaks involving the e_1 exciton state. The real part (square), imaginary part (diamond), and absolute value (circle) amplitude of the e_2, e_1 and e_3, e_1 cross-peaks in the 2D spectrum as a function of population time T are shown. The thin-dashed lines are least-square fitting to the rise component of the real amplitude of the cross-peaks, which yields a $e_2 \rightarrow e_1$ energy transfer time of 190 ± 20 fs and $e_2 \rightarrow e_1$ energy transfer time of 130 ± 40 fs. These values agree well with the population dynamics obtained directly from the dynamical simulations in Fig. 3.

due to the $\widetilde{R}_2^{(\alpha\alpha)}$ energy transfer pathway. Comparing the absolute amplitude to the real amplitude of these cross-peaks, the absolute amplitude exhibits more pronounced beating (due to coherence dynamics), while the rise component representing the energy transfer dynamics is more marked in the real amplitude. Therefore, the real amplitude of the lower diagonal cross-peaks offers a clearer probe to the population dynamics in the system.

The real amplitude of the e_2, e_1 cross-peak shows a rise component due to $e_2 \rightarrow e_1$ population transfer (Fig. 9a). A least-square fit to the simulated real amplitude of the cross-peak reveals a 190 ± 20 fs $e_2 \rightarrow e_1$ exponential population transfer time that describes the rise component (Fig. 9a). This is in good agreement with the 180 fs energy transfer time determined directly from the dynamical simulation in Section 3.2 (Fig. 3). For the e_3, e_1 cross-peak, assuming that the back reaction is negligible, the rise component can be fitted to the conditional probability that describes the sequential $e_3 \rightarrow e_2 \rightarrow e_1$ population transfer

$$G_{e1,e3}(t) = \frac{1}{k_{23} - k_{12}}\left[k_{23}(1 - \mathrm{e}^{-k_{12}t}) - k_{12}(1 - \mathrm{e}^{-k_{23}t})\right],$$

where k_{23} is the $e_3 \rightarrow e_2$ relaxation rate and $k_{12} = 1/190\ \mathrm{fs}^{-1}$ is the $e_2 \rightarrow e_1$ relaxation rate. A least-square fit to the rise component of the real amplitude of the e_3, e_1 cross-peak yields a $e_3 \rightarrow e_2$ population transfer time scale of 130 ± 40 fs (Fig. 9b). This, again, is in agreement with the value of 150 fs obtained from the direct dynamical simulation. Note that we are able to discriminate the $e_2 \rightarrow e_1$ rate from the $e_3 \rightarrow e_1$ rate and thus obtain the complete population dynamics from the simulated 2D spectra. This discrimination is advantageous when considering dynamics in a multichromophoric system and demonstrates the power of 2D electronic spectroscopy.

The lower diagonal cross-peaks also exhibit excitonic quantum beats, and the absolute amplitude of these cross-peaks can also be used as a probe for the coherence dynamics in the system. If the upper diagonal peaks can not be resolved in the 2D electronic spectrum, it is possible that one can use the real amplitude of lower diagonal 2D cross-peaks to determine time scales for energy transfers and then subtract the energy transfer contributions from the time dependence of the absolute amplitude to quantify the coherence dynamics.

4.3. The cross-peaks between e_2 and e_3 exciton states

We now consider the population time-evolution of the cross-peaks involving exciton e_2 and e_3. These cross-peaks exhibit more complicated dynamics because both the $|e_2\rangle\langle e_2|$ and $|e_3\rangle\langle e_3|$ population states are nonstationary and undergo relaxation. In Fig. 10a, we show the time-evolution of the amplitude of the upper diagonal e_2, e_3 cross-peak. The absolute amplitude of this cross-peak exhibits beating and a rapid decay at short T, but no observable dynamics associated with the 190 fs $e_2 \rightarrow e_1$ relaxation, indicating that both the $R_1^{*(\alpha\alpha f)}$ and $\widetilde{R}_2^{*(\alpha\gamma f)}$ excited state

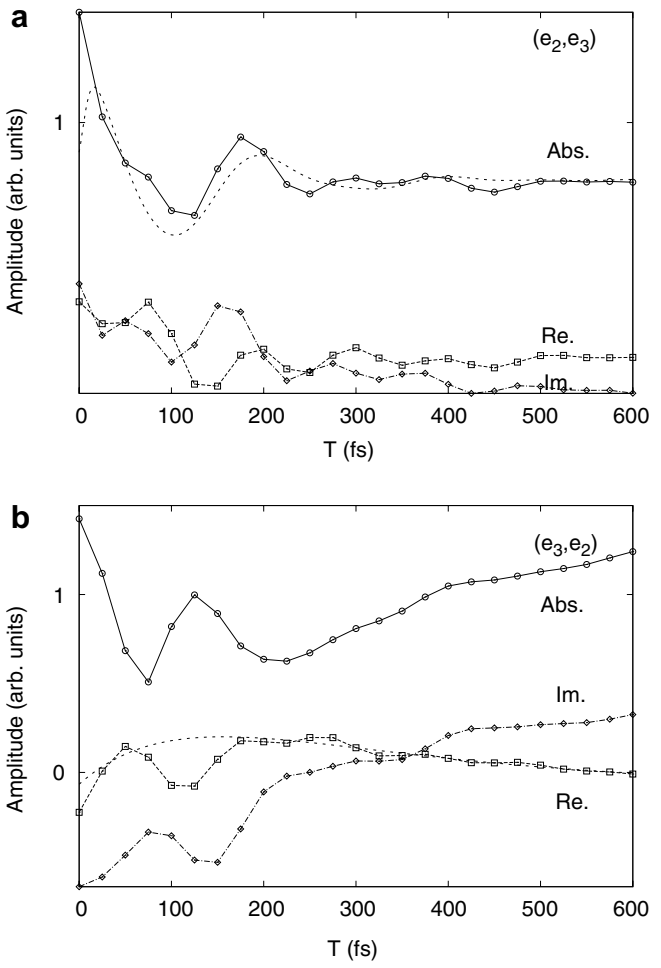

Fig. 10. Population time-evolution of 2D cross-peaks involving e_2 and e_3 exciton states. The real part (square), imaginary part (diamond), and absolute value (circle) amplitude of the cross-peaks in the 2D spectrum as a function of population time T are shown. (a) The evolution of the upper diagonal e_2, e_3 cross-peak. The thin-dashed curve is the real part of the coherence density matrix element $\rho_{23}(t)$ (scaled). (b) The evolution of the lower diagonal e_3, e_2 cross-peak. The thin-dashed curve is the population of e_2 exciton state when the system is initially in the e_3 state, predicted by the kinetic model obtained from least-square fitting in Fig. 7.

absorption contributions to this cross-peak are negligible. This is also consistent with the 2D real spectrum at $T = 0$ (Fig. 5), in which no negative excited state absorption feature is observable at the e_2, e_3 cross-peak. Therefore, the fast decay at short T must be due to the bath relaxation and is related to the decay of the transition frequency correlation functions of the excitations. Nevertheless, the beat can be clearly seen and clearly correlated to the time-evolution of the coherence density matrix element shown as the thin-dashed curve in Fig. 10a.

In Fig. 10b, we show the time-evolution of the amplitude of the lower diagonal e_3, e_2 cross-peak. The time-evolution shows more complicated dynamics; however, the general observations obtained in the previous section still apply. The real amplitude of the cross-peak probes the energy transfer dynamics, now exhibiting a rise component corresponding to the $e_3 \rightarrow e_2$ population transfer and a decay

component corresponding to the subsequent $e_2 \rightarrow e_1$ population transfer. The thin-dashed curve in Fig. 10b shows the conditional probability of finding the system in the $|e_2\rangle\langle e_2|$ population state when the system is initially in the $|e_3\rangle\langle e_3|$ population state predicted by the kinetic model obtained from the least-square fit in Fig. 7. The good agreement of this curve with the real amplitude of the cross-peak confirms that the real amplitude of the lower diagonal cross-peaks probes the population dynamics in the system.

5. Energy transfer and coherence dynamics in the FMO complex

To demonstrate the theoretical modeling on the trimer system presented in the previous section indeed describes experimental signals, we show the cross-peak evolution of 2D electronic spectra measured on the Fenna–Matthews–Olson bacteriochlorophyll (FMO) complex of green sulphur bacteria in this section. Two-dimensional electronic spectra of the Fenna Matthews Olson (FMO) trimer complex isolated from *Chlorobium tepidum* [21] were acquired at a series of 33 population times, T, as described previously [10]. Briefly, we used a home-built Ti:Saph oscillator and regenerative amplifier [28] to produce pulses centered at 800 nm with a FWHM of 35 nm at a repetition rate of 3.4 kHz. The temporal duration of the pulses was determined to be 41 fs FWHM using frequency-resolved optical gating (FROG). Using a beamsplitter and variable delay stage, two beams of equal intensity were focused onto a diffractive optic optimized for the first-order and negative first-order diffraction spots yielding a pattern of four beams in a square geometry [29–31]. The delay time between the first two pulses was controlled precisely by moving pairs of 1 degree fused silica wedges to step the coherence time, τ, in 4 fs increments from -600 to 600 fs [31]. The fourth beam was attenuated and used as a local oscillator for phase-sensitive heterodyne detection and spectral interferometry. The phase of the polarization in the complex plane was determined using pump probe spectroscopy as described by Brixner et al. [5]. The 33 population times sampled were $T = 0$, 10, 20, 30, 40, 50, 65, 80, 95, 110, 125, 140, 155, 170, 185, 200, 220, 240, 260, 280, 300, 330, 360, 390, 420, 450, 480, 510, 540, 570, 600, 630 and 660 fs.

Previous analysis of this data focused primarily on the exciton beating signals apparent in the lowest energy diagonal exciton peak visible in the real part of the third-order material polarization [10]. In this work, we focus instead on the absolute value of the third-order polarization. By analyzing the absolute value, we eliminate any errors that may arise from improper phasing, and as shown above, we improve resolution of quantum beating by leveraging correlation between oscillations in the real and imaginary portions of the response. This improved sensitivity allows observation of quantum beats not only within the main diagonal spectral features, but also within the cross-peak regions.

The signal present in the upper diagonal portion of the spectrum is small and not sufficiently well resolved by our experiment for detailed consideration; therefore, we concentrate only on the lower diagonal cross-peaks in this analysis. We approximate the integral over a circular area centered at the cross-peak using a simple sum of the data points within the region; the accuracy of this simple numerical integration is improved by Fourier interpolation during the analysis by zero padding the data.

The beating pattern observed in the most well resolved cross-peak region, which is due to coupling between excitons 3 and 1, is shown in Fig. 11. To compensate for intensity fluctuations, the data has been normalized to the integrated amplitude of the third diagonal exciton peak because this exciton has a long lifetime of almost 3 ps [32] and does not show the dramatic beating signal previously described in the lowest energy diagonal peak [10]. The rise component of the cross-peak signal results from energy transfer from exciton 3 to exciton 1. We are unable to accurately fit the rise observed in the data because of the oscillations and the overlap with neighboring spectral features; the spectral resolution is especially poor in the absolute magnitude spectra because of the broad extent of the dispersive (imaginary) portion of the response. For both the real part and the absolute magnitude, the apparent rise is too fast ($k > 1/300$ fs^{-1}). While many spectral features exhibit population dynamics and can pollute this measurement, the prominent oscillations on top of this growth component show the coherence beating between the pair of excitons and is far less prone to contamination. In this experiment, the beating signal persists strongly throughout the population time sampled. For

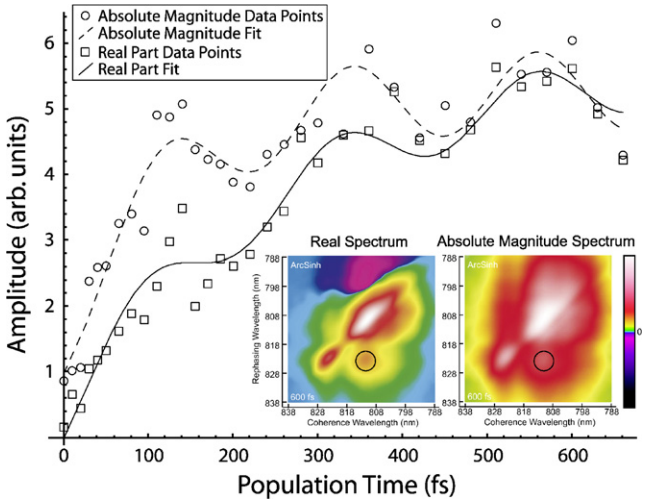

Fig. 11. Beating in *C. tepidum* cross-peak magnitude. The absolute magnitude (circles) and the real part (squares) of the third-order response measured at the lower diagonal cross-peak between excitons 1 and 3 is shown. Energy transfer is evidenced by the rise component, while coherence beating gives rise to the oscillations. The fit (solid line) to the real part reveal a 231 fs (±13 fs) beat period, while the fit (dashed line) to the absolute magnitude shows a period of 220 fs (±8 fs). The predicted beat period is 248 fs. Inset on the graph are two-dimensional spectra of the real and absolute magnitude at $T = 600$ fs with the integrated area for the cross-peak shown by the black circle. Resolution of the absolute magnitude spectra is degraded by the broad imaginary features.

both the real part and absolute value, we fit the oscillatory portion of the data finding periods of 220 fs (±8 fs) and 231 fs (±13 fs), respectively. Calculating the exciton energies from the site Hamiltonian published by Cho et al. [13], we find the expected coherent beating period to be 248 fs. Our experimental data agrees well with the behavior expected from the theory developed previously in both the qualitative character of the energy transfer and the quantitative character of the coherence beating.

6. Conclusions

We have studied theoretically the dynamics and 2D electronic spectroscopy of a linear trimer system using a time-nonlocal non-Markovian quantum master equation formalism [18] and a perturbative scheme [19,20] for the calculation of the 2D spectra. The results confirm the intuition provided by the impulsive limit response functions and further demonstrate that for the linear trimer system investigated in this work, the beats of the upper diagonal peaks in the absolute value spectra provide a direct and quantitative probe for the coherence dynamics in the system, and the time-evolution of the lower diagonal cross-peaks in the real value spectra reveal the population transfer dynamics between exciton states. Combination of the information evaluated from both the upper and lower diagonal cross-peaks thus provides a full understanding of the population and coherence dynamics of the quantum system. We expect the same analysis can be applied to interpret experiments on multichromophoric systems and used to extract population and coherence dynamics when the cross-peaks can be resolved.

In a recent 2D experiment, a lower diagonal cross-peak was resolved in the 2D spectra of the Fenna–Matthews–Olson (FMO) bacteriochlorophyll complex of green sulphur bacteria [10]. The experimental data shows that the time-evolution of this cross-peak exhibits a rise component and long-lasting quantum beat due to excitonic coherence. We expect the analysis presented in this work can be applied to the experimental data to quantify the population and coherence dynamics in the FMO complex.

In this study, we assume that the cross-peaks are well resolved and their amplitude can be determined unambiguously. However, in real experiments the 2D spectrum is usually congested and off-diagonal peaks are not well resolved. In this regard, cross-peak specific techniques utilizing linear polarization of laser pulses or pulse shaping [33–36] to eliminate diagonal peaks in 2D electronic spectra can be valuable tools that will be useful for the direct quantification of the population and coherence dynamics of multichromophoric systems.

Acknowledgement

This work was supported by the Office of Basic Energy Sciences, Chemical Sciences Division, U.S. Department of Energy (contract DE-AC03-76SF000098).

References

[1] S. Mukamel, Ann. Rev. Phys. Chem. 51 (2000) 691.
[2] D.M. Jonas, Ann. Rev. Phys. Chem. 54 (2003) 425.
[3] M. Cho, G.R. Fleming, J. Chem. Phys. 123 (2006) 114506.
[4] J. Hybl, A. Albrecht, S. Faeder, D.M. Jonas, Chem. Phys. Lett. 297 (1998) 307.
[5] T. Brixner, T. Mancal, I.V. Stiopkin, G.R. Fleming, J. Chem. Phys. 121 (2004) 4221.
[6] K. Lazonder, M.S. Pshenichnikov, D.A. Wiersma, Opt. Lett. 31 (2006) 3354.
[7] I.V. Stiopkin, T. Brixner, M. Yang, G.R. Fleming, J. Phys. Chem. B 110 (2006) 20032.
[8] T. Brixner, J. Stenger, H.M. Vaswani, M. Cho, R.E. Blankenship, G.R. Fleming, Nature 434 (2005) 625.
[9] D. Zigmantas, E.L. Read, T. Mancal, T. Brixner, A.T. Gardiner, R.J. Cogdell, G.R. Fleming, Proc. Natl. Acad. Sci. USA 103 (2006) 12672.
[10] G.S. Engel, T.R. Calhoun, E.L. Read, T.-K. Ahn, T. Mancal, Y.-C. Cheng, R.E. Blankenship, G.R. Fleming, Nature 446 (2007) 782.
[11] J. Hybl, Y. Christophe, D.M. Jonas, Chem. Phys. 266 (2001) 295.
[12] S.T. Roberts, J.J. Loparo, A. Tokmakoff, J. Chem. Phys. 125 (2006) 084502.
[13] M. Cho, H.M. Vaswani, T. Brixner, J. Stenger, G.R. Fleming, J. Phys. Chem. B 109 (2005) 10542.
[14] S. Mukamel, Principles of Nonlinear Optical Spectroscopy, Oxford University Press, Oxford, 1995.
[15] W. Zhang, V. Chernyak, S. Mukamel, J. Chem. Phys. 110 (1999) 5011.
[16] M. Cho, T. Brixner, I.V. Stiopkin, H.M. Vaswani, G.R. Fleming, J. Chin. Chem. Soc. 53 (2006) 15.
[17] A.V. Pisliakov, T. Mancal, G.R. Fleming, J. Chem. Phys. 124 (2006) 234505.
[18] C. Meier, D.J. Tannor, J. Chem. Phys. 111 (1999) 3365.
[19] M.F. Gelin, D. Egorova, W. Domcke, J. Chem. Phys. 123 (2005) 164112.
[20] D. Egorova, M.F. Gelin, W. Domcke, J. Chem. Phys. 126 (2007) 074314.
[21] A. Camara-Artigas, R.E. Blankenship, J.P. Allen, Photosyn. Res. 75 (2003) 49.
[22] A.G. Redfield, IBM J. Res. Dev. 1 (1957) 19.
[23] H.-P. Breuer, F. Petruccione, The Theory of Open Quantum Systems, Oxford University Press, Oxford, 2002.
[24] Y.-C. Cheng, H. Lee, G.R. Fleming, J. Phys. Chem. A (2007), doi:10.1021/jp0735177.
[25] W.H. Press, B.P. Flannery, S.A. Teukolsky, W.T. Vetterling, Numerical Recipes in C : The Art of Scientific Computing, Cambridge University Press, 1992.
[26] K.M. Gaab, C.J. Bardeen, J. Chem. Phys. 121 (2004) 7813.
[27] H. Lee, Y.-C. Cheng, G.R. Fleming, Science 316 (2007) 1462.
[28] T. Joo, Y.W. Jia, G.R. Fleming, Opt. Lett. 20 (1995) 389.
[29] J.P. Ogilvie, M.L. Cowan, R.J.D. Miller, Ultrafast Phenomena xiii, Springer-Verlag, Berlin, 2002, pp. 571–573.
[30] M. Cowan, J. Ogilvie, R. Miller, Chem. Phys. Lett. 386 (2004) 184.
[31] T. Brixner, I.V. Stiopkin, G.R. Fleming, Opt. Lett. 29 (2004) 884.
[32] S.I.E. Vulto, M. de Baat, S. Neerken, F. Nowak, H. van Amerongen, J. Amesz, T.J. Aartsma, J. Phys. Chem. B 103 (1999) 8153.
[33] M.T. Zanni, N.H. Ge, Y.S. Kim, R.M. Hochstrasser, Proc. Natl. Acad. Sci. USA 98 (2001) 11265.
[34] D.V. Voronine, D. Abramavicius, S. Mukamel, J. Chem. Phys. 125 (2006) 224504.
[35] D.V. Voronine, D. Abramavicius, S. Mukamel, J. Chem. Phys. 126 (2007) 044508.
[36] E.L. Read, G.S. Engel, T.R. Calhoun, T. Mancal, T.-K. Ahn, R.E. Blankenship, G.R. Fleming, Proc. Natl. Acad. Sci. USA (2007), doi:10.1073/pnas.0701201104.